Fuel 381 (2025) 133440

Contents lists available at ScienceDirect

Fuel

journal homepage: www.elsevier.com/locate/fuel

Full Length Article

Strategies to improve ammonia combustion in a dual fuel marine engine by using CFD

Maria Cristina Cameretti [a], Roberta De Robbio [a,*], Marco Palomba [a], Túlio Zucareli de Souza [b]

[a] Department of Industrial Engineering, University of Naples Federico II, Italy
[b] Mechanical Engineering Institute - Federal University of Itajubá, Brazil

ARTICLE INFO

Keywords:
Dual Fuel
CFD model
Marine Engine
Ammonia
Hydrogen
CO_2 reduction

ABSTRACT

Maritime transportation is currently responsible for delivering most of the world trade, and it still plays a major role in the global economy and pollutant emissions. Due to their heavy loads and long distances, full electrification is generally assumed as an unsuitable pathway, leaving combustion engines as the dominant technology in the marine sector. For a long time, these engines have benefited from the low costs of heavy oils produced from oil refining, but these fuels present a difficult combustion and are associated with significant pollutant emissions and greenhouse gases. Today, carbon-free fuels such as hydrogen and ammonia are gradually getting a foothold in the shipping market.

In the present paper, an investigation on several strategies to improve the oxidation of ammonia is carried out for a dual fuel (DF) medium speed marine engine. A CFD analysis using ANSYS FORTE® code is performed on an improved and more realistic bowl geometry by varying the premixed fuel according to methods validated in previous studies and introducing adequate kinetic mechanisms from the literature. Results show that the sole use of ammonia to replace natural gas, as premixed fuel, leads to incomplete combustion; the increase of diesel fuel can only mitigate this condition, but it cannot be considered as viable solution. Therefore, several blends of ammonia/hydrogen are tested to examine combustion development and pollutant emissions. The addition of hydrogen above 10% to the premixed charge composition demonstrates to promote the oxidation of ammonia and to effectively reduce CO_2 emissions of 84% without a dramatic increase in nitrogen oxides. On the contrary, hydrogen percentages lower than 10% feature a worsening of the combustion of the premixed charge. Finally, the use of a fuel containing nitrogen promote a slight formation of NO_x emissions.

1. Introduction

Currently, it is estimated that over 80 % of the global trade is delivered by ships, putting maritime transportation as one of the major economic sectors in the world [1]. Due to the heavy loads and long distances involved, this sector is mainly dominated by internal combustion engines (ICE), representing 98 % of the merchant fleet [2]. This sector is responsible for about 10 % of all transportation emissions and 2.9 % of total emissions [3], making pivotal to find alternatives that make maritime transportation both economically and environmentally viable. In fact, the shipping industry uses almost exclusively fossil fuels, and presents a 20 % increase in greenhouse gas emissions in the last decade [1]. In this sense, international merchant ships must obey the emission regulations defined by the International Maritime Organization (IMO) [4], which have become stricter over the years [5]. Even though several pathways can be considered for achieving a near zero-carbon scenario, it is expected that combustion engines will maintain for long their domain in naval applications, given their high torque, efficiency, and weight, which fit the demand and architecture of ships [6]. In some cases, electrification is found to be beneficial at lower loads

Abbreviations: BDC, Bottom Dead Center; ATDC, After Top Dead Center; BTDC, Before Top Dead Center; BTE, Brake Thermal Efficiency; CAPEX, Capital Expenses; CFD, Computational Fluid Dynamics; CI, Compression Ignition; DF, Dual Fuel; DOI, Duration of Injection; ER, Equivalence Ratio; GHG, Greenhouse Gas; HRF, High Reactivity Fuels; ICE, Internal Combustion Engine; ID, Ignition Delay; IMEP, Indicated Mean Effective Pressure; IMO, International Maritime Organization; KH-RT, Kelvin-Helmholtz/Rayleigh-Taylor; LHV, Lower Heating Value; LRF, Low Reactivity Fuels; NG, Natural Gas; RANS, Reynolds Averaged Navier-Stokes; RNG, Re-Normalisation Group; ROHR, Rate of Heat Release; RP, Premixed Ratio; SI, Spark Ignition; SOI, Start of Injection; TDC, Top Dead Center.

* Corresponding author.
E-mail address: roberta.derobbio@unina.it (R. De Robbio).

https://doi.org/10.1016/j.fuel.2024.133440
Received 25 January 2024; Received in revised form 31 August 2024; Accepted 13 October 2024
Available online 17 October 2024

[7], but it remains unsuitable for most of the real marine applications [8] given its high-volume requirements and storage capital expenses (CAPEX) [9]. Nuclear power has also been considered for the future of maritime transportation but presents several barriers such as safety issues and technology limitation [10]. Other unconventional systems, such as solid oxide fuel cells, are reported to be potentially suitable for ships as well [11], but still face economical [12] and technical [13] challenges that require further improvements.

Assuming that the most realistic transition towards a more sustainable and efficient shipping industry is the more efficient utilization of fuels in ICEs, many studies and commercial solutions have been proposed in this sense. There is a wide range of scientific approaches being constantly applied to obtain advances in marine engines, including alternative fuels [14], injection techniques [15], control of temperature [16], cogeneration [17], and advanced concepts of combustion [18]. Regarding the latter, dual-fuel operation appears as a potential option for efficient engine operation, being able to reduce the consumption of diesel and heavy oils by partially replacing them with locally available, renewable and/or cheaper fuels [19]. Depending on the fuel, engine and technological characteristics, dual-fuel mode can decrease emissions of certain pollutants, while keeping the original advantages of high performance and low fuel consumption.

Dual-fuel operation with methane/natural gas is a well-established technology, this gaseous fuel is widely used as a partial replacement fuel for fossil fuels in marine engines [20] thanks to the reduced CO_2 emissions compared to diesel [21]. It is necessary to point out that the study of the behaviour of the engine supplied with NG provides the basis for the analysis of other fuels. Some outcomes are reported in Table 1.

Hydrogen is a promising fuel for renewable transportation, including maritime applications [27,28]. However, despite its high potential, challenges like production costs, transportation, storage [29], and NO_x emissions due to high combustion temperatures must be addressed [30]. As summarized in Table 2, hydrogen in maritime dual-fuel engines can either increase [31,32] or decrease [33] BTE and generally increases ID [32,34] like NG. While NO_x emissions tend to rise due to higher combustion temperatures [35], pollutants like CO, HC, and PM usually decrease [32,36], except when combustion efficiency drops [35,37].

Ammonia is suitable for spark ignition (SI) engines due to its high octane number (around 130 [39]) and anti-knock properties [40], but its low flame speed and high auto-ignition temperature pose challenges for compression ignition (CI) engines, often requiring pilot diesel injection [41]. Ammonia as a low-reactivity fuel (LRF) in CI engines can lead to different outcomes depending on the engine operating conditions. As expected for any carbon-free fuel, ammonia utilization leads to CO and CO_2 emissions reduction. In many cases ammonia combustion often causes higher NO_x, N_2O, and NH_3 emissions. However, strategies like high-pressure direct injection, advanced pilot injection, and optimized injector positioning can reduce these pollutants [9]. Research on a 2.44L Caterpillar 3401 diesel engine showed that advanced pilot diesel injection timing could minimize greenhouse gas emissions (GHG), despite higher quantities of unburned NH_3, HC, N_2O, and CO compared to diesel single-fuel operation [42]. Advanced injection is also cited as a useful strategy by Shin and Park [43], compensating the slow ammonia flame speed and resulting in lower emissions of unburned NH_3 and N_2O, at the cost of increased NO_x. Using a higher equivalence ratio is also pointed out as an option for improving the premixed combustion of ammonia, while leading to a tradeoff between lower N_2O and higher NO_x [44]. The overall behavior of ammonia dual-fuel engines is summarized in Table 3 for various marine engines in terms of combustion, performance, and emissions parameters. All studied references for marine engines indicated that ammonia leakage in the exhaust gas may occur to some extent, and that increased N_2O emissions are almost always observed. NO_x emissions, on the other hand, presented strong variations according to the conditions in which the combustion takes place. Rodriguez et al. [40] observed a non-linear behavior between ammonia concentration and NO_x emissions, with the optimal point lying in an intermediate substitution fraction.

Ammonia is a hydrogen carrier, therefore, to overcome the limits of its flammability they can be well combined for combustion. However, also in case of NH_3/H_2 blends researchers are more focused on their combustion in SI engines. In particular, to control their reactivity several strategies, such as variation of ammonia share, variable valve timings and oxygen enrichment were experimentally investigated [48,49]. On the other hand, only few works focused on the use of these blends in CI ignition engines [50] and even less on dual fuel with diesel [51,52]. Wang et al. [51] investigated the effects of the compression ratio to engines performance for a fixed percentage of NH_3-H_2 (70 %/30 %). The enhancement of the compression ratio improved the power performance while as expected NOx and N_2O emissions increase. Anyway, an effective injection timing can achieve a level of NOx emissions that meet the Tier III emission standards. Qian et al. [52] experimentally demonstrated that the addition of hydrogen leads to an increase of maximum heat release and in-cylinder pressure inhibiting soot emissions, at the expense of NOx emissions at medium and high load. At low load the beneficial effect of hydrogen on mixture oxidation diminished.

The authors of this work have widely studied both experimentally and numerically dual fuel combustion applied to automotive engines [53–61]. Starting from the use of NG, new models have been implemented and validated to describe also hydrogen and its blends with NG. Given their expertise the same methodology is used in this work to conduct an in-depth investigation into the dual-fuel combustion of ammonia in a Wärtsilä 20DF marine engine at medium load. Moreover, numerical CFD simulations with the ANSYS FORTE® code are carried out on several mesh grids featuring shapes more compliant to those typical of pistons used in marine engines. After a mesh sensitivity analysis, the results on the new geometry are compared with those performed on the simplified presented in ref. [6] to demonstrate the effective improvement in the description of the in-cylinder phenomena with a more realistic bowl shape. In addition, after a proper validation of the spray model the results are validated against experimental data using NG. Two cases i.e., 100 $\%CH_4$ and 40 $\%CH_4$-60 $\%H_2$, are used as reference to evaluate the complete substitution of the premixed fuel with ammonia. In all cases, an injection of n-dodecane (n-$C_{12}H_{26}$), as diesel oil surrogate, is used to activate combustion as foreseen in dual fuel

Table 1
Summary of trends for different parameters from works using NG as fuel.

Type of engine	Operational conditions	BTE	ID	CO	CO_2	NO_x	PM	HC	CH_4	Ref.
2-stroke low speed dual-fuel marine diesel engine, 1 cylinder, bore x stroke 400 x 2315 mm	97–99.4 % NG, energy based, at 95.6 rpm, high load	↑	↑	–	–	↓	–	–	–	[22]
4-stroke dual-fuel marine engine, 4 cylinders, bore x stroke 190 x 210 mm	60–80 % NG, energy based, at 1000 rpm, full load, using different diesel-rapeseed oil methyl ester blends	↓	↑	↓	–	↓	↑	↑	↑	[23]
Four-stroke diesel engine, single cylinder, bora x stroke 86 x 83 mm	89.8 % NG, at 1500–2500 rpm	↓	–	↑	↓	↓	–	↓	–	[24]
Four-stroke diesel engine, single cylinder, bore x stroke 86 x 83 mm	0–86 % NG, at 1500–2500 rpm, low to high load	↓	–	↑	–	↓	–	↑	–	[25]
YC6K dual fuel engine adapted for dual-fuel operation, bore x stroke 129 x 155 mm	81.1–84.0 % NG, mass based, at 1228–1800 rpm, low to full load	↑	–	↓	–	↓	–	↓	–	[26]

Table 2
Summary of trends for different parameters from works using hydrogen as fuel.

Type of engine	Operational conditions	BTE	ID	CO	CO_2	NO_x	PM	HC	Ref.
4-stroke W20DF Wärtsilä diesel engine, 6 cylinders, 1440 kW @ 1000 rpm	12 % pilot diesel and 88 % H_2/CH_4 mixtures, with 0–100 % H_2 concentration, energy based, at 1000 rpm, medium load	–	–	↓	↓	↑	–	↓	[6]
4-stroke 4190ZLC-2 diesel engine, 4 cylinders	0–15 % H_2 fraction, energy based, at 1000 rpm, medium to full load, rapeseed methyl ester/water blends as pilot fuel	↑	–	↓	–	↑	–	↓	[31]
4-stroke diesel engine, 4 cylinders, 220 kW @ 1000 rpm	0–6 % H_2 fraction, energy based, at 1000 rpm, low to full load, cottonseed and rapeseed methyl esters as pilot fuels	↑	↑	↓	–	↑	–	↓	[32]
2-stroke heavy-duty 7RT-flex82T engine, 7 in-line cylinders, 31640 kW @ 80 rpm	0–10 % H_2 fraction, energy based, at 80 rpm, full load	↓	–	–	↓	–	–	–	[33]
2-stroke Detroit Diesel Corporation 12 V-71TI, 12 cylinders, 503 kW @ 2300 rpm	0.05–2.83 % H_2 fraction, volume based, at 657–2053 rpm, idle to full load	–	–	↓LL ↑ML↓HL	↓	↓LL↑HL	↑LL↓HL	–	[35]
4-stroke Deutz A12L 714 diesel engine, 12 cylinders, 112 kW @ 1800 rpm	0–7.77 % H_2 fraction, energy based, at 1500 rpm, low load				↓	↓	↑	↓	[37]
2-stroke heavy-duty 5G70ME-C9.5-GI engine, 10225 kW @ 70 rpm	5 % pilot diesel and 95 % H_2/CH_4 mixtures, with 0–50 % H_2 concentration, mass based, at 70 rpm, full load	–	–	–	↓	↑	↓	–	[38]

LL – Low load
ML – Medium load
HL – High load

Table 3
Summary of trends for different parameters from works using ammonia as fuel.

Type of engine	Operational conditions	BTE	ID	CO	CO_2	NO_x	PM	HC	N_2O	NH_3	Ref.
2-stroke low-speed marine diesel engine, 19.8 compression ratio, bore x stroke 34 x 160 cm	90–99 % NH_3, energy based, at 157 rpm, low to high load	=DI↑PI	–	–	↓	↓DI↑PI	–	–	↑	↑	[9]
4-stroke MAN D2840LE V10 diesel engine, 10 cylinders, 320 kW @ 1500 rpm	0–90 % NH_3, energy based, at 1500 rpm, full load	↓	–	↓HS ↑MS↓LS	↓	↑HS ↓MS↑LS	–	–	↑	↑	[40]
4-stroke Wärtsilä DF32 diesel-natural gas dual-fuel engine, 6 cylinders,	72.16–92 % NH_3, energy based, at 750 rpm, low to medium load	–	–	↓	–	↓	–	–	↑	–	[44]
2-stroke WinGD RT-flex 50DF dual-fuel diesel engine, bore x stroke 500 x 2050 mm	85–95 % NH_3, energy based, at 102 rpm, low to high loads, RSAJI mode	↑	↑	–	–	↓	–	–	–	↑	[45]
2- stroke EX340EF marine diesel engine, 6 cylinders	0–80 % NH_3, energy based, at 143 rpm, high load	–	↑	↓LS↑HS	↓	–	–	–	↑LS↓HS	–	[46]
Diesel engine, 17.5 compression ratio, bore x stroke 95 x 102 mm	0–97 % NH_3, energy based, at 1000 rpm	–	–	–	↓	↓DI↑PI	–	–	↑	↑	[47]

DI – Direct injection
PI – Port injection
HS – High substitution fraction
MS – Medium substitution fraction
LS – Low substitution fraction

concept. Therefore, the kinetic mechanism for the diesel fuel and the one for the oxidation of both ammonia and hydrogen are merged.

The partial oxidation of such fuel suggested to test two different strategies for effective use of ammonia while limiting emissions:

1) increasing the high reactivity fuel (HRF) supply to better sustain the flame;
2) the addition of hydrogen to the premixed charge to improve ammonia weak flammability.

The former solution demonstrated not only to increase carbonaceous emissions, but it is not completely effective as unburned ammonia is still obtained in the exhaust. The second one allows to achieve a complete ammonia oxidation and an impressive reduction of CO_2 for mixture with a 20 % hydrogen contribution. It is demonstrated that a reduced addition of hydrogen leads to a worsening of performance. To obtain an improvement the percentage must be above 10 % value. Finally, A slight enhancement of NO_x emission is obtained with the use of NH_3.

2. Computational modelling

The numerical calculations are performed with the ANSYS FORTE® code on a domain that reproduce the naval engine Wärtsilä 20DF whose characteristic data are shown in Table 4. In a previous paper [6] based on literature data [62], the authors simulated a medium load operating point at 1000 rpm to validate the 3D models and to investigate performance and polluting emissions by fueling the dual fuel engine with methane/hydrogen mixtures with different compositions using a simplified bowl geometry. In the present paper, ammonia, known to be more easily available than hydrogen, is used as a low-reactivity fuel and a new bowl profile is designed (Fig. 1) to approach a shape consistent with that of a commercial marine engine [63].

Table 4
Engine specifications and operating conditions.

DF, 4-stroke, turbocharged, 6 cylinders in line, 4 valves (W20)	
Stroke [cm]	28
Bore [cm]	20
Disp. Volume [cm^3]	8796
CR [-]	13.4:1
Engine speed [rpm]	1000
Gross IMEP [bar]	10
Diesel injection pressure [bar]	1700
Diesel injection timing [°BTDC]	15
Intake pressure [bar]	1.85

The CFD simulations are carried out on a computational domain consisting of a 40 degrees sector including the bowl and the cylinder; the injector has nine holes, and the domain can be assumed as axisymmetric.

The simulations focused exclusively on the closed valve phases, ranging from the Intake Valve Closing at −215° ATDC to the Exhaust

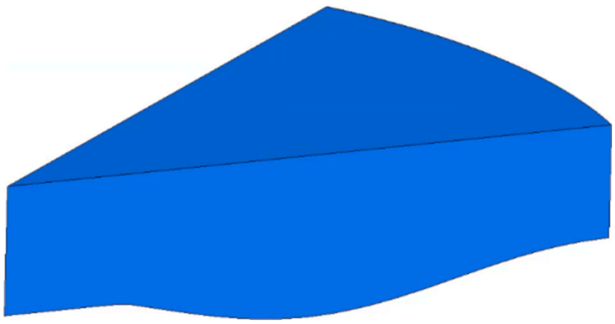

Fig. 1. New designed geometry.

Valve Opening at 145° ATDC.

The unsteady Reynolds-Averaged Navier-Stokes (URANS) equations are used to model the flow field employing a modified version of the SIMPLE iterative algorithm [64] to solve the governing equations, utilizing a two-step iterative process to determine flow field variables. The turbulence effects are simulated via the Renormalization group k-epsilon (RNG k-ε) model [65].

To describe combustion process ANSYS FORTE® directly interfaces with ANSYS Chemkin-Pro solver via a Turbulence Kinetics Interaction model which deals with chemical mechanisms. In the previous studies concerning natural gas and hydrogen or their blends, the well-established GRIMECH mechanism was merged with the scheme proposed by Ranzi et al. [66] for n-dodecane; anyway, the merged mechanism does not foresee a specific chain of reactions for the oxidation of ammonia. For this reason, the Otomo kinetic mechanism [67] is introduced and merged with the already mentioned scheme for diesel fuel leading to a final mechanism consisting of 152 species and 2593 reactions. Both GRIMECH and Otomo mechanisms include a set of reaction for the calculation of NO_x. Additionally, Ansys Forte uses the Dynamic Cell Clustering (DCC) technique to groups similar cells into clusters to optimize the chemical calculations by solving them only once per cluster [68].

For the wall heat transfer assessment, the model by Han and Reitz [69] included in the code is used.

One of the main issues of dual fuel combustion is the correct description of the break-up process of the liquid jet. As clearly noticeable from Tables 1, 2 and 3, ignition delay is affected by the presence of a gaseous fuel in the bulk mixture and may vary depending on its composition. Therefore, a sensitivity analysis to spray features was performed to achieve the optimal results in terms of IMEP. Spray atomization and droplet breakup of solid-cone are modeled by the Kelvin-Helmholtz/Rayleigh-Taylor (KH /RT) hybrid breakup model [70]. It is based on the KH breakup model which is applied within the breakup Length from the nozzle exit, while the RT model is applied to predict the secondary break-up. The primary breakup generates new droplets r_c from parent ones r_p and the radius change of the droplets are governed by the time scale of breakup τ_{KH} which is given by:

$$\tau_{KH} = \frac{3.726 C_{KH} r_P}{\Lambda_{KH} \Omega_{KH}}$$

Where C_{KH} is the Time Constant of KH breakup, Λ_{KH} is the wavelength of the fastest growing wave which leads to the breakup of droplets, Ω_{KH} is its growth rate.

Similarly, the RT model foresees a time scale for secondary breakup τ_{RT} which is given by:

$$\tau_{KH} = \frac{C_{RT}}{\Omega_{RT}}$$

The analysis of spray development led to set the values of Time Constant of KH breakup (C_{KH}) and Time Constant of RT breakup (C_{RT}) equal to 9.5 and 1, respectively.

Finally, the vaporization of spray droplets was modeled using the discrete multi-component (DMC) fuel-vaporization model [71].

2.1. Mesh sensitivity analysis

The mesh sensitivity analysis is performed to optimize the computational time and to ensure the reliability of the results referred to the new presented geometry. The several grids are built using the FORTE® sector mesh generator, they are composed mainly by square elements, their sizes and performance are listed in Table 5. In Fig. 2 the comparison of the number of cells and in-cylinder pressure are reported for dual fuel NG/diesel operating condition presented in ref. [6].

In particular, the three grids feature a refinement across the TDC but only the second and the third grids present very similar outcomes in terms of pressure and Indicated Mean Effective Pressure (IMEP) values with only 1 % difference and close to that of the experimental reference case [62]. Therefore, given the lower number of cells, mesh 2 is chosen as the most appropriate to provide consistent calculations with minimum time requirements.

2.2. Comparison between two bowl profiles

Due to the lack of information about a real bowl shape for this kind of application, the first numerical studies [6] were conducted on a basic square shape geometry, while in Fig. 3 a more realistic shape of the bowl is now presented. The details of the two bowls and grids are displayed in Fig. 3.

As it is possible to observe at the TDC, the new mesh is characterized by more uniform cells in terms of shape and dimension in the whole domain since both bowl and squish regions are considered as a unique layering zone. On the contrary, the old mesh presents stretched cells in the squish region due to the reduced cells layering, while in the bowl the number of cells remains constant over the entire calculation. It is important to notice that the two geometries feature the same displacement and compression ratio, and both mesh grids have nearly the same number of cells as reported in Table 6.

The reason behind the necessity of a bowl profile change is deductible from the streamlines inside the cylinder in Fig. 4. As expected at 10°BTDC, right after the injection event, the flow field is affected only by the injection itself. As a matter of fact, usually combustion chambers used for marine applications are called "quiescent" since the mixing of the liquid fuel is provided only by the high velocity of the jet introduced by the injector and not by any swirl motion. Also, the high velocity leads to the formation and propagation of vortices in the radial direction. Such propagation is influenced by the shape of the bowl, as clearly observable at the TDC. Consequently, n-$C_{12}H_{26}$ contours in Fig. 5 show a more realistic distribution of the vapour fuel for the simulation with the new grid, given the absence of the high concentration near the cylinder head; this convinced the authors to carry on the numerical studies on this geometry.

3. Test cases

Table 7 lists the test cases presented in this study. RP is the primary fuel energy share ratio expressed in percentage following Equation (1); ER_{prem} and ER_g are the equivalence ratios of the primary premixed charge and of the global mixture, respectively; DOI is the duration of

Table 5
Mesh sensitivity analysis.

Mesh n°	Min. number of cells	Peak pressure [bar]	Max. average temperature [K]	IMEP [bar]
Mesh 1	4 702	66.6	1535	7.59
Mesh 2	11 760	101.4	2101	10.09
Mesh 3	28 224	102.6	2113	9.99

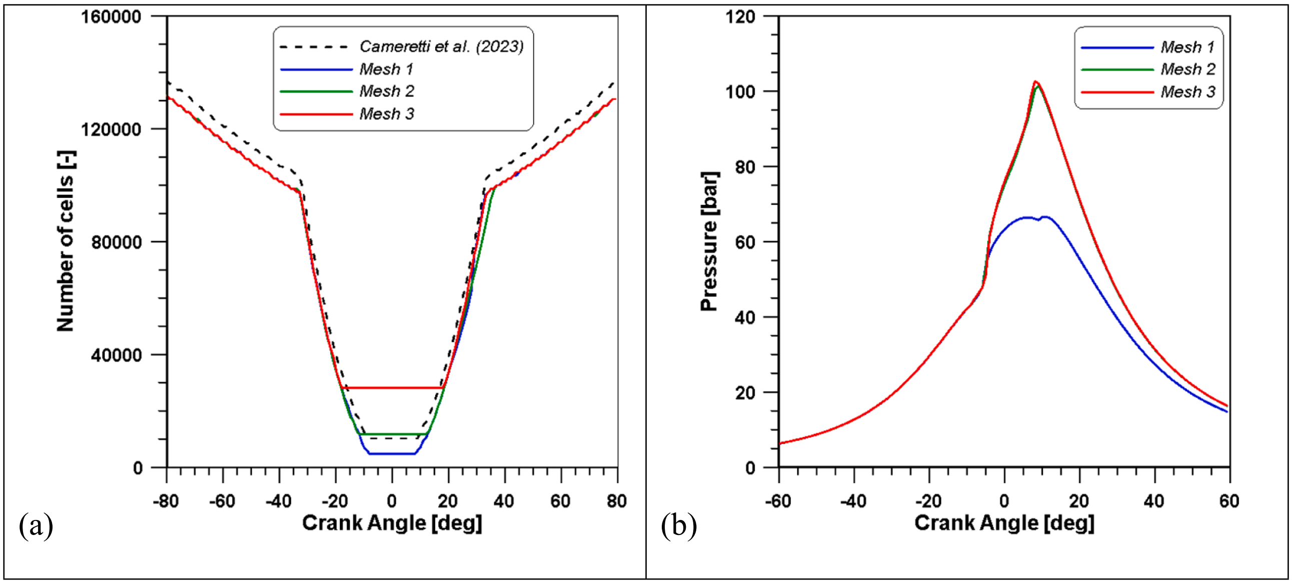

Fig. 2. Mesh sensitivity analysis including: (a) number of cells, (b) in-cylinder pressure.

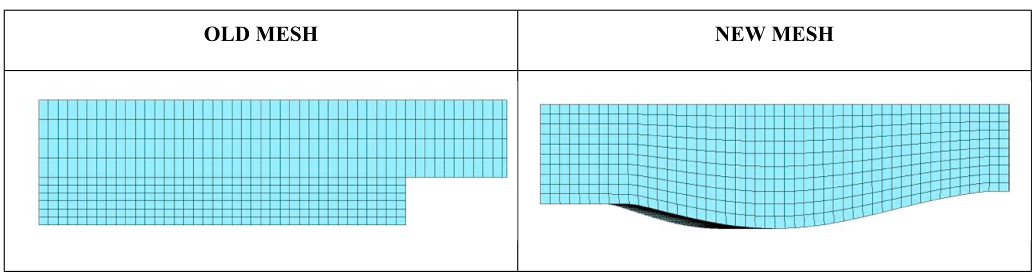

Fig. 3. Comparison of the two mesh grids at the TDC.

Table 6
Maximum and minimum number of cells for the two grids.

Number of cells	Old Mesh	New Mesh
TDC	10 176	11 760
BDC	184 224	178 752

diesel injection.

The first case listed in Table 7 is named "base" because, as anticipated, the 100 % methane case is the one used to validate the models against the experimental data [62] and it represents the reference for the new performed cases.

The operating point considered is at medium load based on an IMEP level equal to 10 bar, speed of 1000 rpm, start of injection (SOI) equal to 15°BTDC and injection pressure of 1700 bar (see Table 4). A constant wall temperature of 450 K is applied across all surfaces for all simulations, while the initial conditions are derived from the 1D simulation depending on the composition of the fuel. The in-cylinder initial pressure and temperature are around 1.605 bar and 362.5 K, respectively.

$$RP = \frac{m_{pf}LHV_{pf}}{m_{pf}LHV_{pf} + m_{sf}LHV_{sf}} \quad (1)$$

For Case#1, the same conditions are set, but a methane/hydrogen blend, respectively 40 % and 60 %, is used as LRF. As anticipated, the simulations of the first two cases make use of the GRIMECH 3.0 as reaction mechanism for the oxidation of methane and hydrogen, but such scheme is merged with the reduced kinetic scheme proposed by Ranzi et al. [66] to reproduce n-dodecane oxidation as well. The baseline and #1 cases were already presented in a previous work [6] using the square bowl geometry; however, as already explained and illustrated in section 2.2, in this paper new results are performed and presented with reference to the new bowl geometry.

From cases #2 to #4 pure ammonia and from cases #5 to #7 ammonia/hydrogen blends are utilized as premixed fuel. As already mentioned, with the addition of ammonia it is necessary to use a different kinetic mechanism for the premixed charge since the GRI-MECH 3.0 does not foresee a specific chain of reactions for the oxidation of this species. To this aim Otomo kinetic mechanism [67] is introduced and merged with the same scheme for n-dodecane [66].

The motivations behind this simulations' pattern are based on the subsequent outcomes presented in the results' section. Indeed, two strategies are followed with the aim to limit carbon fuels while keeping an adequate level of performance.

Case#2 is characterized by the same diesel fuel amount, almost the same energy input and equivalence ratio of the premixed fuel to evaluate the performance of the engine when only ammonia is supplied.

In Cases#3 and Case#4, while keeping the same ER_{prem} of Case #2, the efficiency of ammonia flame propagation is improved by increasing the liquid fuel amount (from 50 to 110 and 180 mg/cycle, respectively); to this aim the duration of the injection must be increased as well to keep constant the level of injection pressure (1700 bar in Table 4). As a matter of fact, this strategy has the only aim to analyze the combustion development as the increase of carbonaceous fuel, obviously, is not viable solution.

Therefore, to promote combustion of ammonia, in Cases #5, #6 and #7 increasing percentages of hydrogen in blend with ammonia are tested (5, 10 and 20 %). In fact, a fuel characterized by a high reactivity

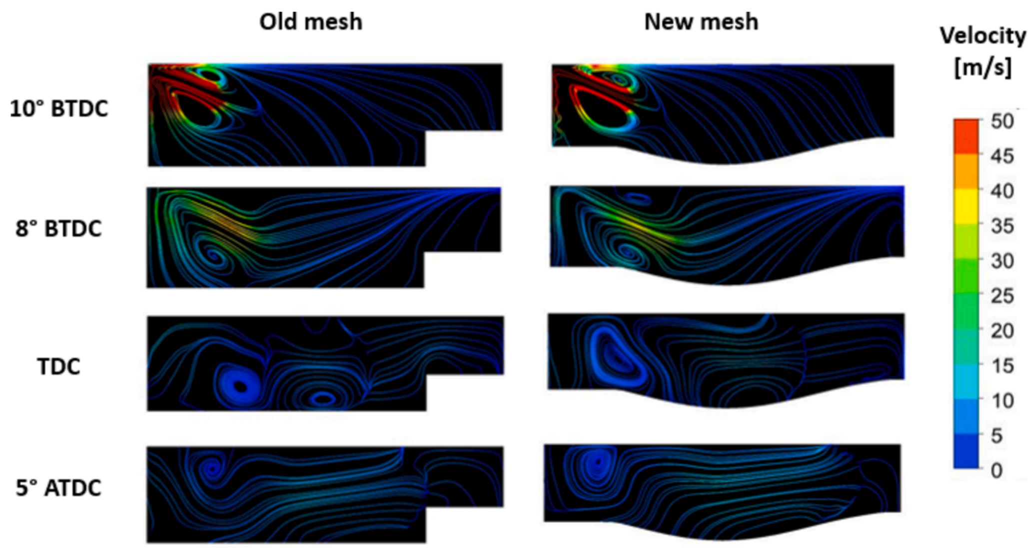

Fig. 4. Streamlines for the two mesh grids.

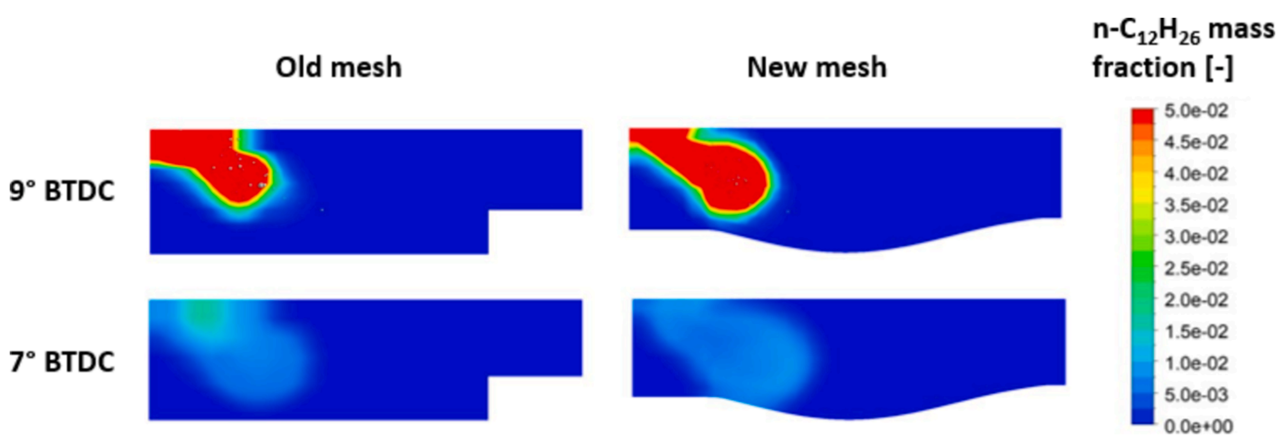

Fig. 5. N-dodecane distributions for the two mesh grids.

Table 7
Test cases.

Case	Premixed blend	Energy Input [kJ]	RP [%]	Fuel mass [mg/cycle]			ER_{prem}	ER_g	Diesel mass [mg]	DOI	Kinetic mechanism
				CH_4	H_2	NH_3					
Base	CH_4	18.5	88	328	–	–	0.43	0.50	50	1.5° CA	GRIMECH 3.0 [6]
1	CH_4/H_2 (60 % – 40 %)	18.5	88	131	81	–	0.41	0.47	50	1.5° CA	GRIMECH 3.0 [6]
2	NH_3	18.7	88	–	–	887	0.44	0.50	50	1.5° CA	Otomo [67]
3	NH_3	21.3	77	–	–	887	0.44	0.57	110	3.2° CA	Otomo [67]
4	NH_3	24.4	67	–	–	887	0.44	0.65	180	5.4 °CA	Otomo [67]
5	NH_3/H_2 (95 % – 5 %)	18.7	88	–	7	842	0.44	0.50	50	1.5° CA	Otomo [67]
6	NH_3/H_2 (90 % – 10 %)	18.7	91	–	14	798	0.44	0.50	50	1.5° CA	Otomo [67]
7	NH_3/H_2 (80 % – 20 %)	18.7	91	–	28	709	0.43	0.49	50	1.5° CA	Otomo [67]

such as hydrogen can be beneficial for the combustion process of ammonia.

4. CFD results

In Fig. 6 the results of Case #2 (only ammonia premixed with air) are illustrated together with the baseline case, Case #1, and the experimental data [62].

From a first comparison between the base case and the experimental outcomes in Fig. 6.a and b, it is possible to observe that the three-dimensional model is adequately capable to reproduce the behaviour of the real engine, especially considering the perfect reproduction of ignition phase. Indeed, the trends of rate of heat release (ROHR) present the first peak and its rise almost overlapped.

In Case#1 the partial substitution of methane in the premixed charge with a fuel featuring a higher laminar flame speed, such as hydrogen,

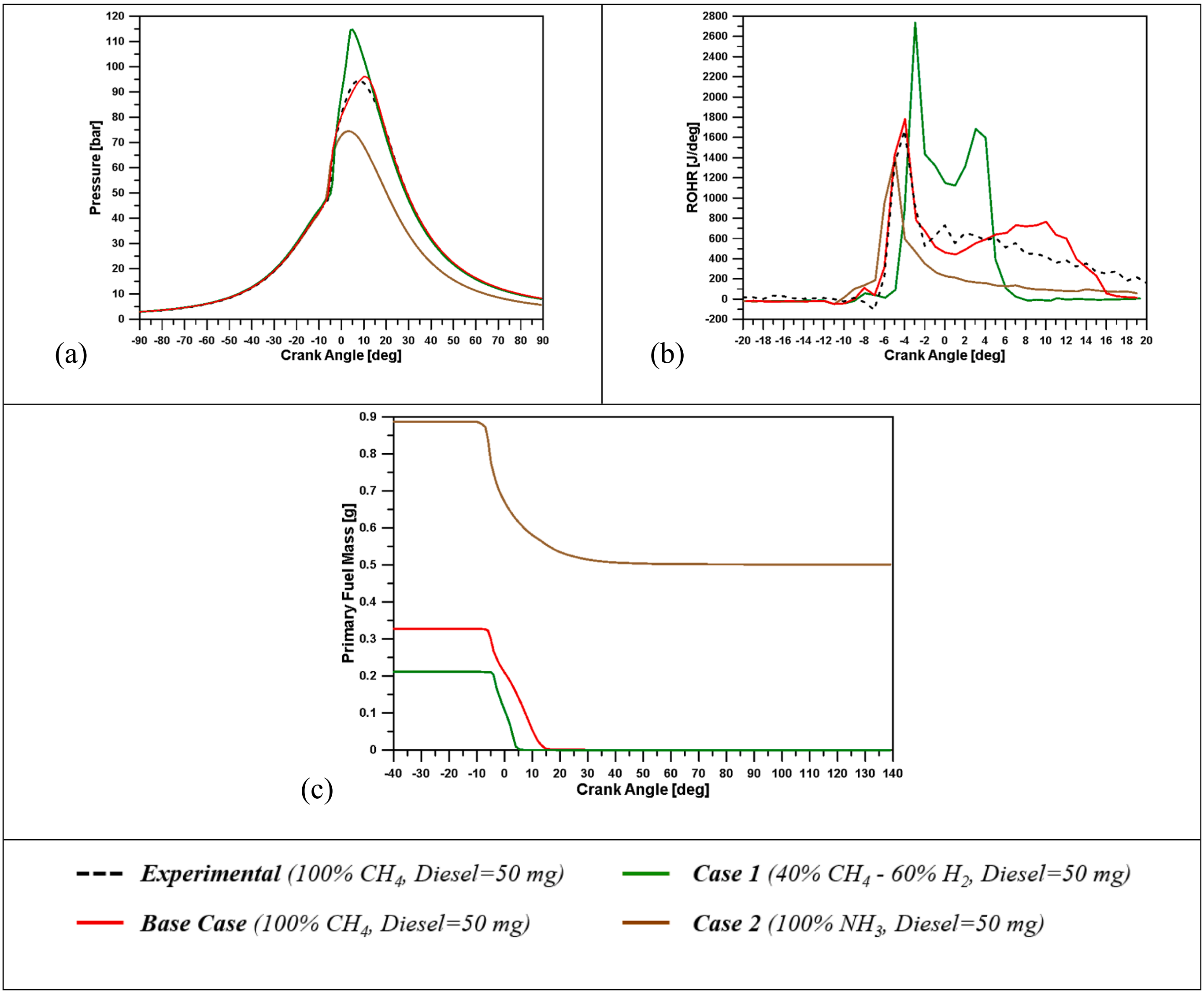

Fig. 6. In-cylinder pressure, ROHR, Primary fuel mass: Case 2 compared with Experimental, Base and Case 1.

leads to a faster combustion process as demonstrated by the higher peak pressure and the quick decrease of the ROHR curve. However, such feature is compensated by H_2 higher ignition temperature with respect to methane, as demonstrated by the longer delay of the premixed charge in the ROHR; such characteristic was already pointed out in Table 2.

Finally, Case#2 outlines outcomes completely different from the previous ones. The pressure level is significantly lower, implying an unsatisfying performance of the engine when the premixed fuel is pure ammonia. The ROHR presents only the first peak, probably due to the first combustion oxidation sustained mainly by the pilot diesel fuel. On the contrary, the Base Case and Case#1 show a second ROHR peak after the TDC, indicating an effective resumption of combustion of the mixture due to the higher flammability of methane and hydrogen.

Fig. 6.c displays the consumption of the primary fuels that for each simulated case are: pure methane, a blend of methane and hydrogen, and pure ammonia, respectively. The Base Case and Case#1 claim a complete oxidation of all considered fuels, while in Case #2, although the higher mass of gas fuel (NH_3) introduced and the consequent a slightly higher ER_{prem}, the oxidation process is considerably inefficient, causing higher presence of this species in the exhaust.

As a matter of fact, the presence of unburned ammonia in the exhaust should be absolutely avoided to prevent damages to the exhaust system and environment. With the aim to improve ammonia fuel reactivity and complete its oxidation, the following possible solutions are examined:

- Injection of a greater amount of diesel oil in the cylinder
- Addition of hydrogen to ammonia in the mixture

4.1. Increase of pilot fuel amount

The enhancement of pilot amount is an attempt to improve the oxidation process of NH_3. Indeed, it was already demonstrated in ref. [56] that the pilot injection not only acts as the activator of ignition, but it can play a role in sustaining the combustion, as well. To evaluate the effects of this strategy, Cases#2, #3 and #4 are discussed, where only the amount of injected diesel is increased while the energy input of ammonia is kept unaltered as reported by the constant values of ER_{prem} in Table 7. However, the global equivalence ratio is increased to obtain better combustion condition at the expenses of the RP value from the carbon-free fuel. As already stated, such solution is not viable in current times, where a reduction of carbonaceous emission is mandatory, but still, it is important to investigate this case study as well, since it is one of the main strategies adopted in real applications to overcome reduced performance at low loads [25,72].

In Fig. 7, a comparison of the three cases with pure ammonia in the premixed charge is reported together with the baseline Case to assess the changes of performance and combustion behavior. The effect of the increased diesel supply appears evident both in terms of combustion development and species. Pressure and temperature in Fig. 7.a and 8.b show an increasing trend with the increase of diesel fuel; this is expected due to the added energy input. On the contrary, the development of combustion described by the ROHR is of particular interest (Fig. 7.c).

By enhancing the n-dodecane mass more than two or three times, a longer ignition delay occurs. It is necessary to recall that the duration of the injection is extended to keep the same level of injection pressure. Indeed, in Fig. 8, the spray and n-dodecane distributions, reported at 8°BTDC, show that the vaporization of diesel fuel in Case#2 is already over, but it is still occurring in Case#3, while in Case#4 the pilot injection is still ongoing, and it is likely that the increased amount of liquid fuel lowers the temperature near the jet axis slowing the overall auto-ignition phase. Anyway, once the combustion is initiated, the whole oxidation process is greatly accelerated as evidenced by the strong rise peak (Fig. 7.c). In addition, the smoother second bump typical of the premixed charge in dual fuel combustion is not present.

Furthermore, in Fig. 9 the mass' trends of the main species are displayed in grams to track and compare the absolute quantities present inside the cylinder in the different cases during the computations. Firstly, the ammonia consumption (Fig. 9.a) highlights that the increase of pilot fuel can effectively promote the consumption of the premixed fuel. However, a complete oxidation is not reached even with a quantity more than three times higher. This may be due to the n-$C_{12}H_{26}$ distributions in Fig. 8, as diesel vapor remains near the jet axis; therefore, it is able to sustain NH_3 oxidation only in that region, while far from the spray direction ammonia weak flammability does not allow its total consumption.

The carbon dioxide graph in Fig. 9.b, as expected, highlights increased emissions when more diesel fuel is provided. Also, by looking at Fig. 9.c, this emission can be even higher considering the incomplete oxidation of the pilot fuel evidenced by the presence of carbon monoxide for Cases#3 and #4; maybe the strong augmentation of diesel hampers its own oxidation. Nevertheless, by analyzing only the baseline case and Case#2 in which the diesel fuel amount is the same (Table 7) and its oxidation is complete as shown in Fig. 9.c, the emissions of CO_2 are drastically reduced because this species cannot be produced by a carbon-free fuel such as ammonia.

Finally, nitrogen oxides in Fig. 9.d demonstrate a decreasing trend with the increase of diesel fuel. The presence of more diesel mass favored the combustion of ammonia, reducing the NO_x value and the comparison with the base case is successful having higher peak

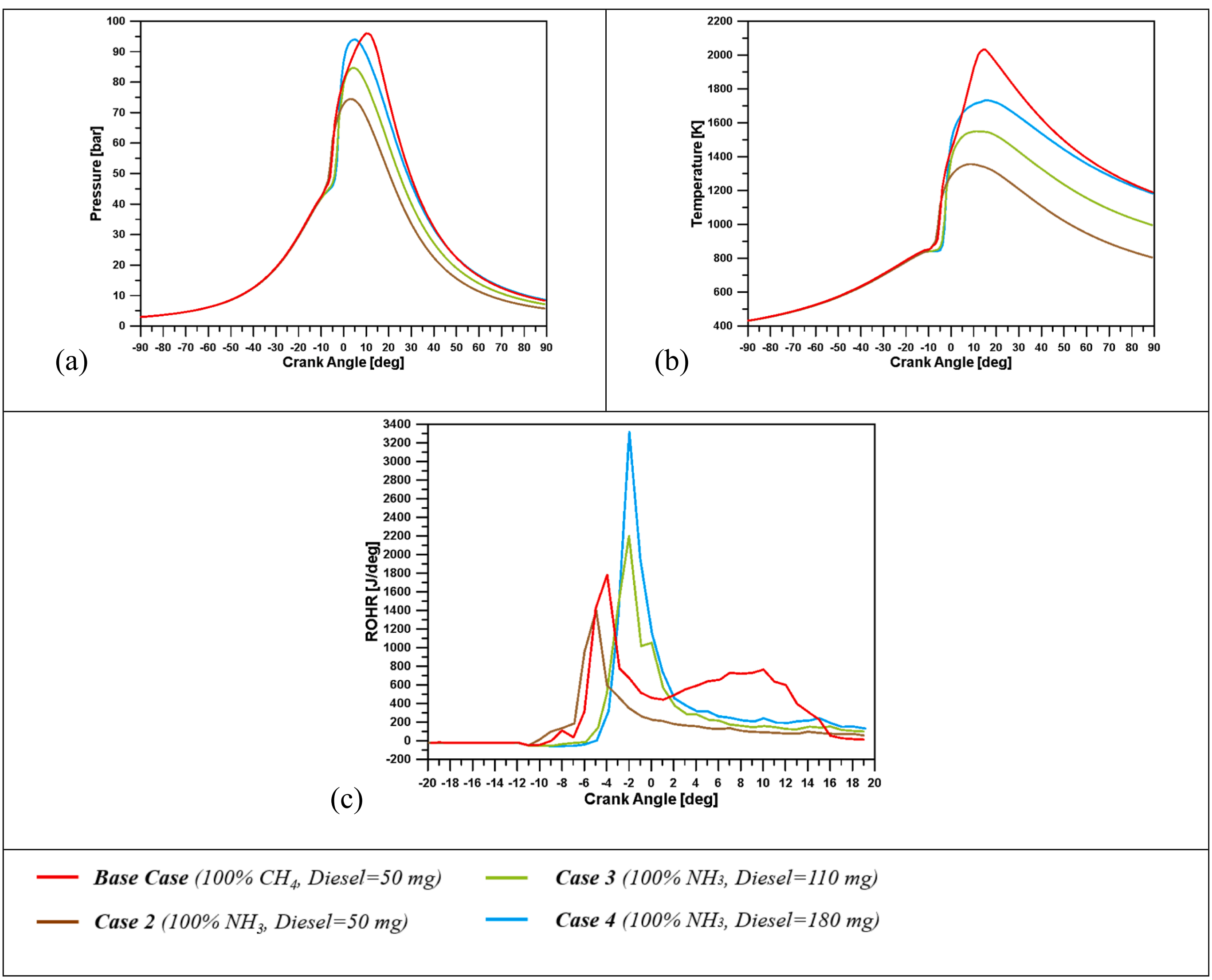

Fig. 7. In-cylinder pressure, temperature, ROHR for Cases Base, 2, 3 and 4.

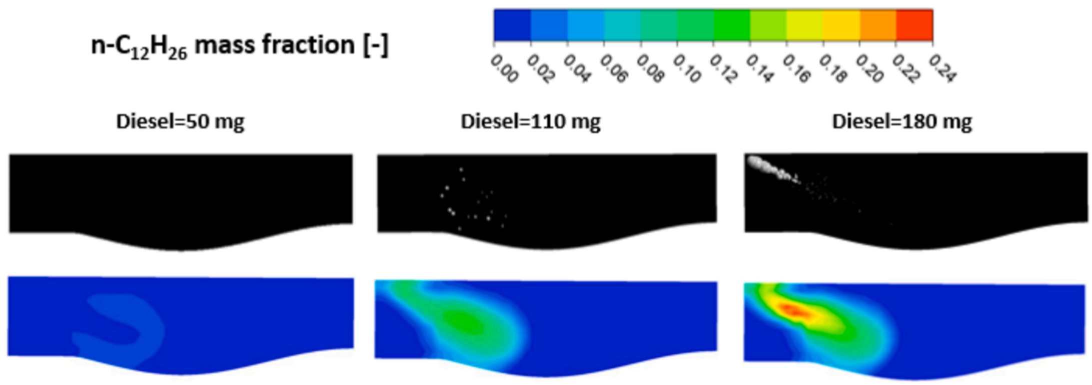

Fig. 8. Distributions of spray and n-dodecane vapour for Cases #2, #3 and #4 at 8°BTDC.

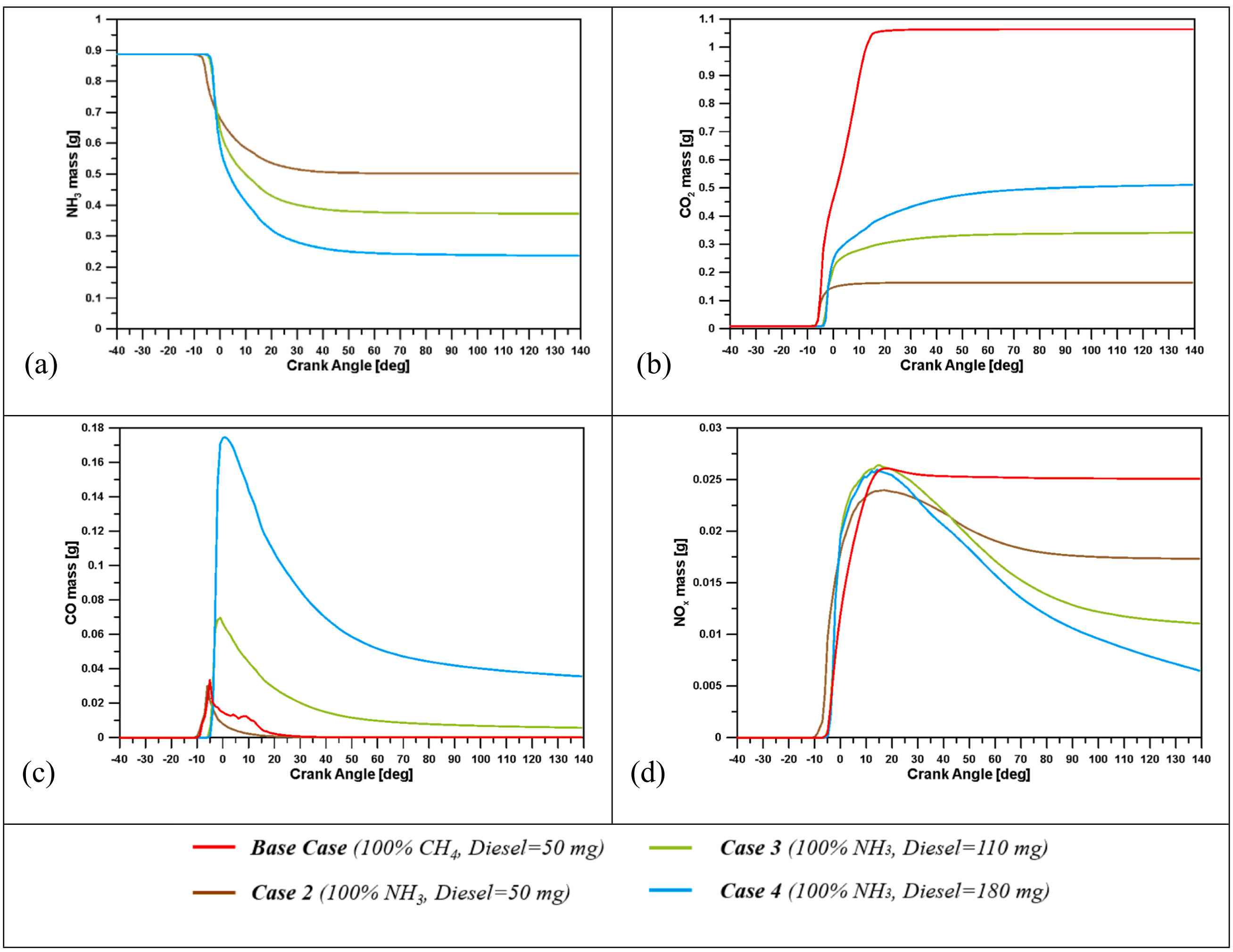

Fig. 9. Mass of NH_3, CO_2, CO, and NO_x for Cases Base, 2, 3 and 4.

temperature values (Fig. 7. b).

The results obtained from the previous strategy evidence that the increase of pilot fuel provides a better sustaining of the flame only in proximity of the jet location, but more importantly the target of emissions of carbonaceous reduction is not achieved and it cannot be achieved following this path. For these reasons, the second approach aims at improving the flammability of the premixed charge, relying on another carbon-free fuel characterized, on the contrary, by excellent combustion properties: hydrogen.

4.2. Addition of hydrogen

As second option, hydrogen replaces a portion of ammonia, leaving the quantity of diesel unchanged at 50 mg (Table 7). In Fig. 10 the in-cylinder pressure, temperature and the ROHR of Cases#5, #6 and #7 are compared with the Base Case (pure methane) and Case#2 (pure ammonia).

As observable in Fig. 10.a and b, the introduction of different hydrogen amounts leads to different results. The mixture with the lowest

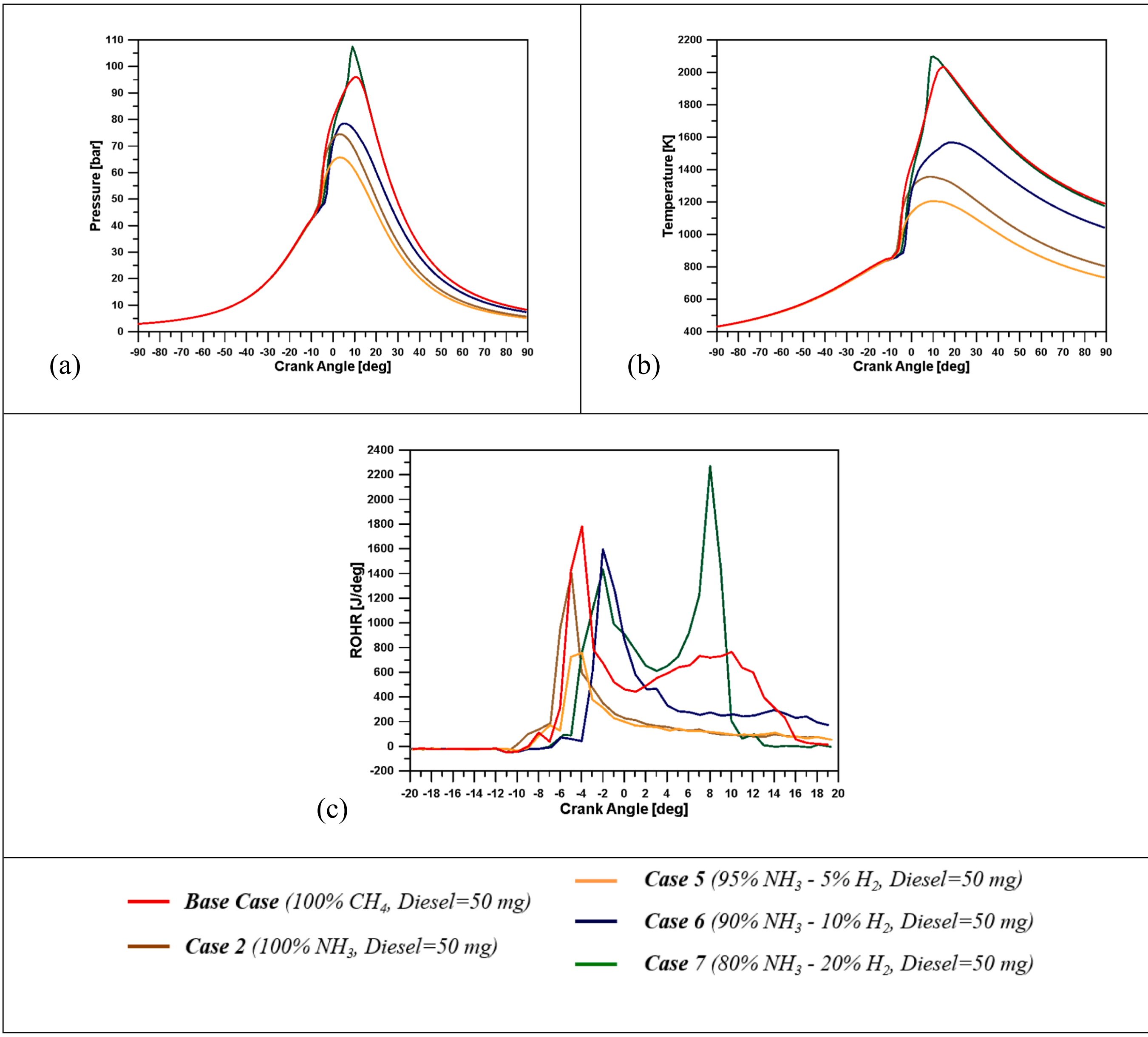

Fig. 10. In-cylinder pressure, temperature, ROHR for Cases Base, 2, 5, 6 and 7.

percentage (5 %) causes a worsening of performance with respect to pure ammonia. In this case, hydrogen amount is very small, and it could act as a diluent and inhibit mixture oxidation. Instead starting from a 10 % of hydrogen supply increased pressure and temperature levels are attained; when the contribution of H_2 reaches 20 % they are even higher than the baseline case. Again, the ROHR in Fig. 10.c presents a longer ignition delay of diesel fuel. As matter of fact, hydrogen features a high diffusivity, and this may interfere with the formation of diesel/air charge responsible for the initialization of combustion. However, the rise to first peak is slightly retarded in the Case#6 compared to Case#7 suggesting that a maximum delay is obtained around 10 %. In addition, concerning the oxidation of the premixed charge, it is evident that with a 10 % H_2 contribution combustion improves and for 20 % a strong acceleration occurs as demonstrated from the already discussed second spike, even higher than the first one.

All these results have implications in terms of emissions as illustrated in Fig. 11. The introduction of hydrogen proves to be insufficient for the burning of the bulk ammonia in Case #5 (5 % of H_2) and Case #6 (10 % of H_2) as observed in Fig. 11.a. However, it is likely that in the former case the presence of hydrogen exacerbates NH_3 consumption; while when H_2 contribution rises to 10 % a significant improvement is achieved but still insufficient. On the contrary, with 20 % of hydrogen, a complete consumption of ammonia is finally obtained.

Moreover, it must be considered that hydrogen is introduced as part of primary fuel and its efficient oxidation should be ensured as well. Instead in Fig. 11.b it is interesting to notice that in Case #2 hydrogen is produced during the first combustion phase because it is present in the long chain of reactions of both ammonia and n-dodecane; anyway, it can be completely converted. Conversely, Case#5 shows a more significant bump that seems to be detrimental for H_2 consumption itself since almost the same amount of this species can be found in the exhaust. For Cases#6 and #7 the same considerations already observed for ammonia can be made, and this is in accordance with the increasing temperature levels inside the cylinder, as also demonstrated in Fig. 12 where temperature contours are reported.

The carbon emissions in Fig. 11.c and .d highlight an important result: except for Case #5, a H_2 supply higher than 10 % drastically reduces CO_2 emissions compared to the baseline case without affecting

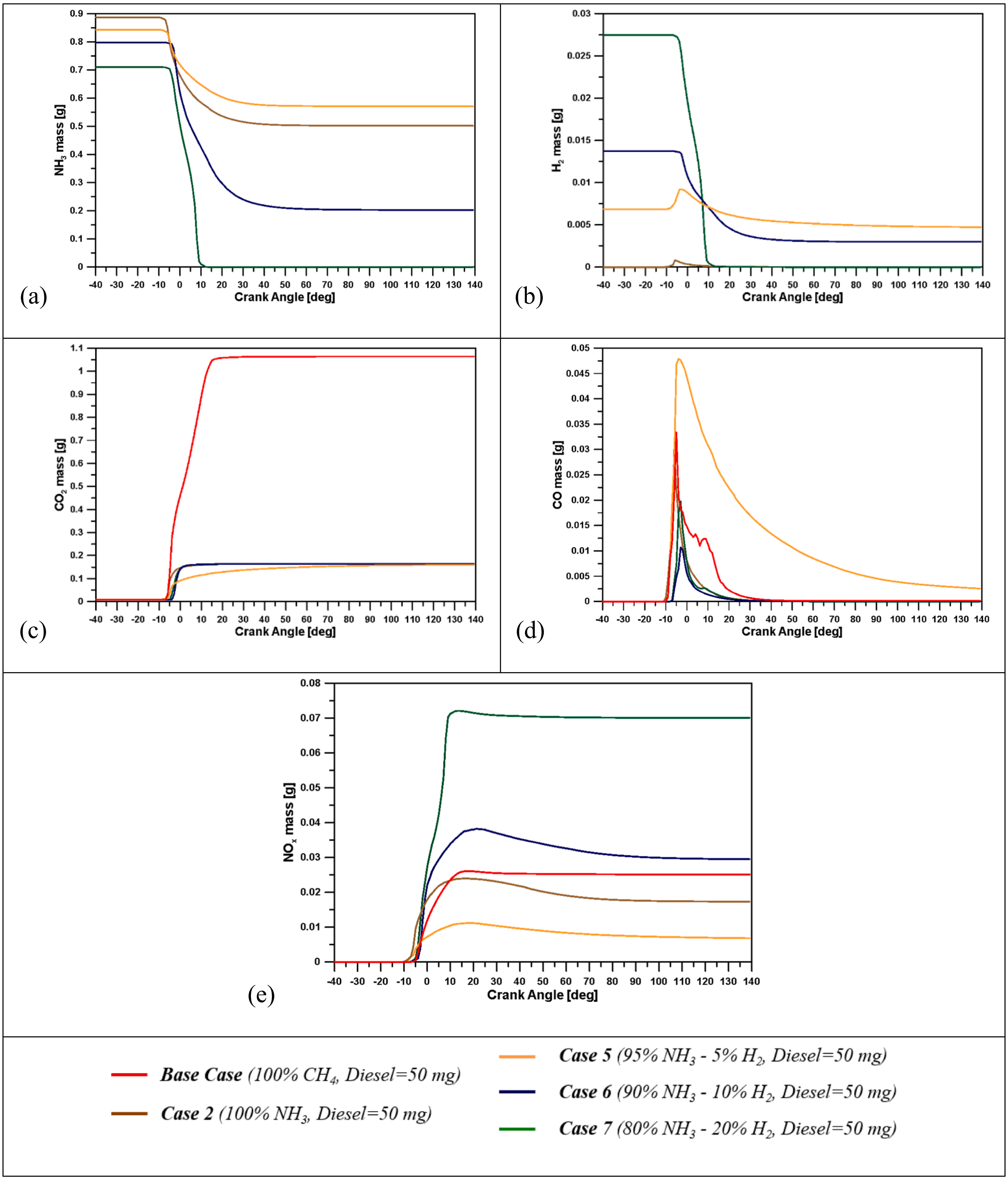

Fig. 11. Mass of NH_3, H_2, CO_2, CO, and NO_x for Cases Base, 2, 5, 6 and 7.

diesel fuel oxidation as confirmed by the complete conversion of CO. This demonstrates that this solution can be a real opportunity for the reduction of GHG in marine applications. Nevertheless, when it comes to hydrogen in ICEs, nitrogen oxides can be a critical issue. Indeed, by looking at Fig. 11.e NO_x emissions are higher than the baseline case. Anyway, it must be considered that usually in these applications after-treatment systems are used, while in the study presented in this work they are not accounted for.

From Figs. 12 to 15, distributions of the main critical variables are reported. Temperature contours in Fig. 12 confirm the considerations made for the ROHR (Fig. 10.c), i.e. the increase of temperature due to the heat release is retarded when H_2 is added to the premixed fuel. Peak values over 2500 K are achieved in all cases but NO emissions are driven also by the extension of high temperature regions (Fig. 13). It is evident from temperature distributions that for Case#5, the high reactivity zone is mainly driven by n-dodecane oxidation, and it does not involve the whole bulk mass due to the scarce flammability of the mixture. While for Case#7 at 20°ATDC even the near wall mass has been involved in the

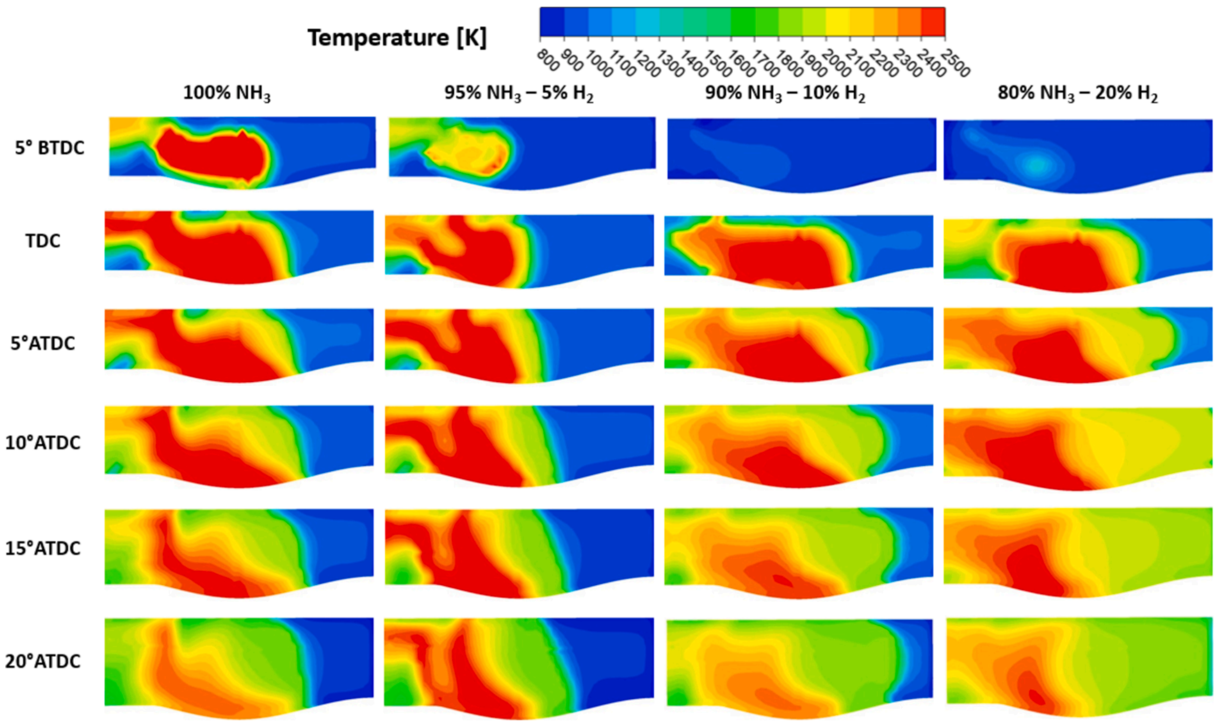

Fig. 12. Temperature distribution at different crank angle for Cases #2, #5, #6 and #7.

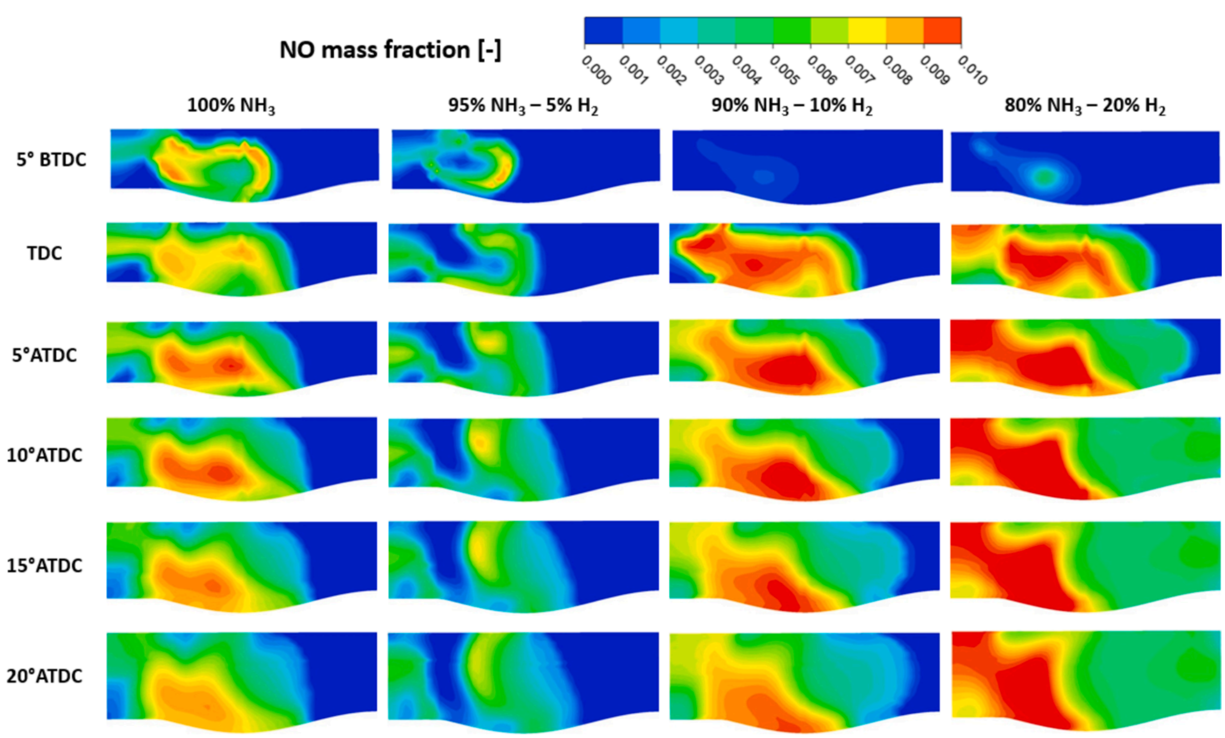

Fig. 13. Nitrogen oxides distribution at different crank angle for Cases #2, #5, #6 and #7.

combustion process since, as already observed in Fig. 11.a and b, NH_3 and H_2 oxidation is complete. Ammonia and hydrogen distributions in Figures 14 and 15 lead to the same conclusions: unburned species are located near the wall region where the flame has not reached out.

Finally, Fig. 15 shows for Case #5 (5 % of H_2) the already mentioned hydrogen production, which is detected along the jet axis, it is likely due to the incomplete oxidation of n-dodecane, since Cases#2 and #6 feature an inefficient conversion of NH_3 as well but the high concentration of H_2 region is not formed.

4.3. Comparison and discussion

Table 9 lists the results in terms of performance and emissions for all analyzed cases. The columns with ammonia and hydrogen slips refer to

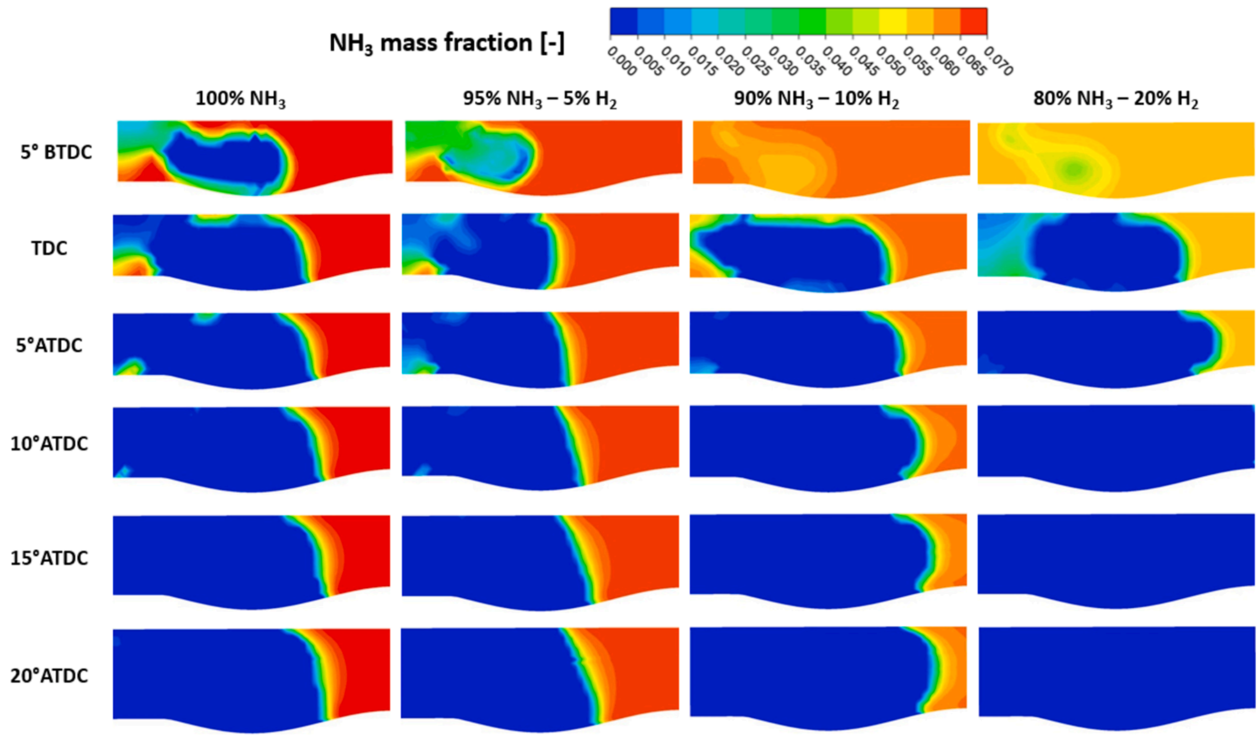

Fig. 14. Ammonia distribution at different crank angle for Cases #2, #5, #6 and #7.

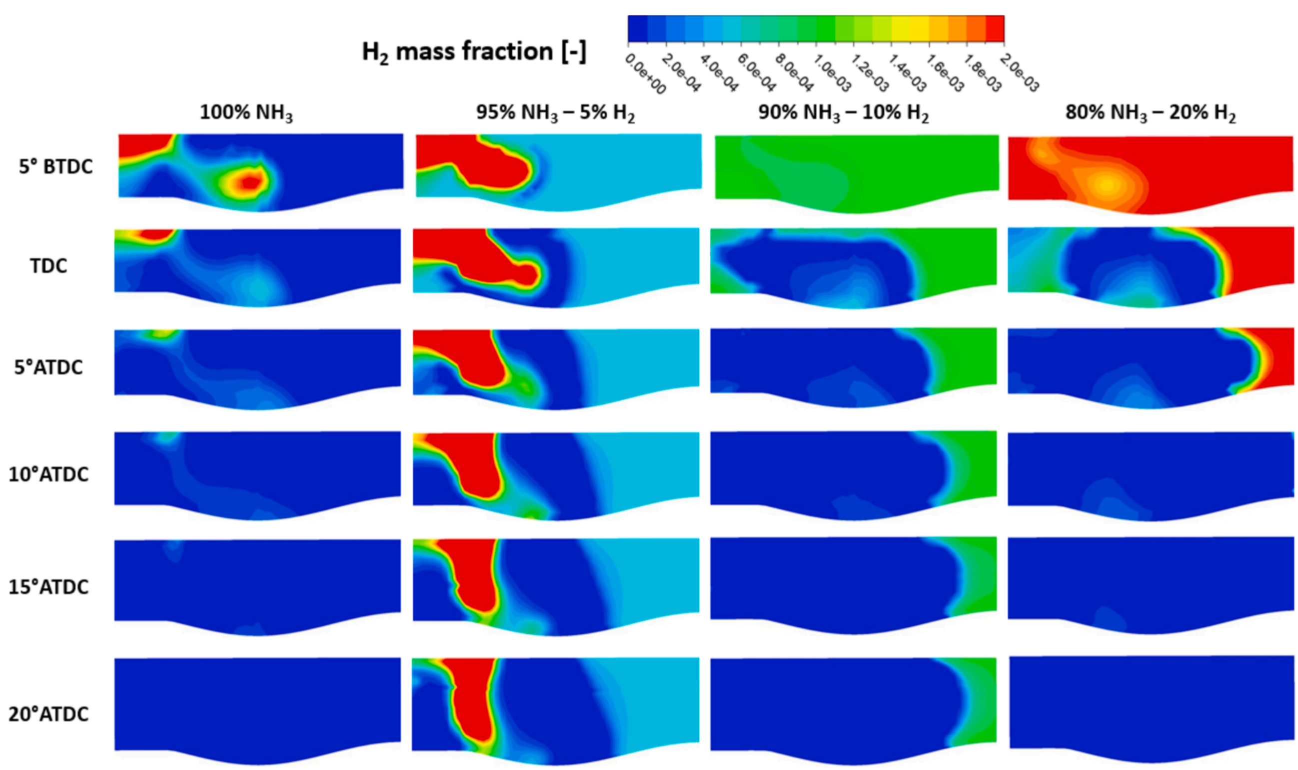

Fig. 15. Hydrogen distribution at different crank angle for Cases #2, #5, #6 and #7.

the percentage of unburned species with respect to the only introduced mass of that species.

The baseline case has been calibrated not only to obtain the same combustion development but also the same performance as the experimental reference operating point. Indeed, a value close to 10 bar of IMEP as reported in ref. [62] has been achieved. The aim of the fuel change is to reduce emissions while maintaining a similar level of performance as the original engine, as demonstrated in Case#1 where 40 % of methane is substitute with hydrogen. Such goal is attained with a IMEP level of 10.2, a reduction of CO_2 and without excessively increasing NO_x emissions.

On the contrary, the total substitution of the primary fuel with pure

Table 9
Performance and emissions' results.

Case	Premixed blend	IMEP[bar]	CO_2[ppm]	CO[ppm]	NO_x[ppm]	NH_3 slip[%]	H_2 slip [%]	Combustion efficiency	Thermal efficiency
Base	CH_4	10.6	7.89×10^4	9.47	1.86×10^3	–	–	0.99	0.51
1	CH_4/H_2	10.2	4.16×10^4	2.88×10^{-2}	2.67×10^3	–	0	0.99	0.49
2	NH_3	5.3	1.25×10^4	8.03	1.32×10^3	56	–	0.50	0.25
3	NH_3	7.8	2.59×10^4	4.16×10^2	8.31×10^2	42	–	0.67	0.32
4	NH_3	10.4	3.86×10^4	2.65×10^3	4.60×10^2	27	–	0.82	0.37
5	NH_3/H_2 (95 %-5%)	4.12	1.23×10^4	1.89×10^2	5.18×10^2	68	68	0.40	0.19
6	NH_3/H_2 (90 %-10 %)	8.23	1.26×10^4	1.10	2.26×10^3	25	22	0.78	0.39
7	NH_3/H_2 (80 %-20 %)	10.7	1.27×10^4	4.12×10^{-2}	5.44×10^3	0	0	0.99	0.50

ammonia (Case #2) exacerbates the engine outputs: IMEP, combustion efficiency and thermal efficiency are halved, while emissions are not significantly reduced. More importantly, more than 50 % of ammonia is not able to burn.

The enhancement of diesel pilot (Cases #3 and #4) improves the performance up to achieve the original IMEP. Since major amount of C-based fuel is introduced, it is expected that carbon dioxide emissions strongly increase, but against the expectations this does not occur due to the overall inefficient oxidation that, on the contrary, enhances CO in the exhaust of two and three orders of magnitude, respectively. For the same reason, NO_x emissions are lower than the previous cases, although a slight improvement of NH_3 conversion is present.

Despite the already discussed worsening of results when a supply of 5 % from hydrogen is provided, the progressive contribution of hydrogen up to 20 % (Case#7) is beneficial under all aspects:

- Performance in terms of IMEP, combustion and thermal efficiency are kept as the original engine ones.
- The issues of ammonia and hydrogen slips are overcome.
- CO_2 emissions are reduced by 84 %.
- Such reduction is the consequence of the real decrease of carbon in the fuel since the lower CO concentration in the exhaust demonstrates the complete oxidation of n-dodecane.

Finally, as it is possible to observe from Table 9 nitrogen oxides are increased, but it must be recalled that in this work the aftertreatment systems are not taken into account.

5. Conclusions

In this work, ammonia is assessed as premixed fuel in a Wärtsilä medium-speed, four-stroke marine engine. Originally, the engine was developed for natural gas and diesel dual-fuel operation. After the validation of the model against experimental data, a blend of methane/hydrogen is simulated, and a mesh sensitivity analysis is carried out on a computational domain consistent with real naval piston shapes.

Firstly, the study examines the combustion process of diesel and ammonia, the latter totally substitute the primary fuel. For this reason, a new kinetic mechanism is introduced to analyze the formation of some pollutants and greenhouse gas as well. When ammonia operates under similar conditions as the baseline natural gas engine, in terms of diesel amount and injection strategy, poor engine performance is observed. The combustion efficiency drops from 99 % to 50 % due to the low propagation speed of the premixed flames, leading to a significant unburned NH_3 escape (56 %).

In this sense, two strategies are examined: increase of pilot diesel and hydrogen addition to the ammonia mixture.

- The first solution foresees a higher energy input from diesel. The aim is to sustain the flame through the premixed charge and to ensure a high combustion efficiency. In all cases the injection pressure of diesel is kept at 1700 bar, and since the injected mass increases the injection duration must be longer as well. This leads to completely different combustion development with a higher ignition delay and a faster oxidation process. However, results showed that improvements can be obtained but only in proximity of the jet axis, and they are still unsatisfying in terms of performance and especially emissions.
- The second approach is to replace part of the ammonia with hydrogen to improve the flammability of the overall premixed charge. Three percentages are tested: 5 %, 10 % and 20 %. The smallest contribution of H_2 case presents a worsening of combustion even with respect to the baseline case (CH_4/diesel), but the subsequent enhancement of hydrogen allows to achieve a complete oxidation of entire primary fuel in the case with 80 % NH_3 and 20 % of H_2, with both ammonia and hydrogen slips being reduced to zero. In addition, IMEP, combustion and thermal efficiency reach acceptable values for this application. Finally, the use of carbon-free species as fuel demonstrates a significant reduction of CO_2 (84 %) and almost null CO emissions, without dramatically affecting NO_x.

Future works will be focused on the extension of other engine operating points to validate the CFD model and check whether the mixtures used are effective in other engine conditions.

CRediT authorship contribution statement

Maria Cristina Cameretti: Supervision, Project administration, Methodology, Funding acquisition, Data curation, Conceptualization. **Roberta De Robbio:** Writing – review & editing, Writing – original draft, Formal analysis, Data curation. **Marco Palomba:** Visualization, Software, Investigation, Data curation. **Túlio Zucareli de Souza:** Writing – original draft, Software, Investigation, Data curation.

Declaration of competing interest

The authors declare that they have no known competing financial interests or personal relationships that could have appeared to influence the work reported in this paper.

Acknowledgements

This research of University of Naples Federico II was supported by EU funding within PNRR project 'Centro Nazionale per la Mobilità Sostenibile' (CUP E63C22000930007), Mission 4, Component 2.

Data availability

Data will be made available on request.

References

[1] UNCTAD. Review of maritime transport 2022 - navigating stormy waters. 2022.

[2] Bilousov I, Bulgakov M, Savchuk V. Modern marine internal combustion engines. Cham: Springer International Publishing; 2020. 10.1007/978-3-030-49749-1.

[3] Sæther SR, Moe E. A green maritime shift: Lessons from the electrification of ferries in Norway. Energy Res Soc Sci 2021;81:102282. https://doi.org/10.1016/j.erss.2021.102282.

[4] Eyring V, Isaksen ISA, Berntsen T, Collins WJ, Corbett JJ, Endresen O, et al. Transport impacts on atmosphere and climate: Shipping. Atmos Environ 2010;44:4735–71. https://doi.org/10.1016/j.atmosenv.2009.04.059.

[5] Godet A, Nurup JN, Saber JT, Panagakos G, Barfod MB. Operational cycles for maritime transportation: A benchmarking tool for ship energy efficiency. Transp Res D Transp Environ 2023;121:103840. https://doi.org/10.1016/j.trd.2023.103840.

[6] Cameretti MC, De Robbio R, Palomba M. Numerical analysis of dual fuel combustion in a medium speed marine engine supplied with methane/hydrogen blends. Energies (Basel) 2023;16:6651. https://doi.org/10.3390/en16186651.

[7] Hayton M. Marine electrification is the future: a tugboat case study. In: Smart Rivers. Singapore: Springer Nature Singapore; 2023. p. 868–79. https://doi.org/10.1007/978-981-19-6138-0_77.

[8] Bhattacharyya R, El-Emam RS, Khalid F. Climate action for the shipping industry: Some perspectives on the role of nuclear power in maritime decarbonization. E-Prime - Advances in Electrical Engineering, Electronics and Energy 2023;4:100132. https://doi.org/10.1016/j.prime.2023.100132.

[9] Zhou X, Li T, Wang N, Wang X, Chen R, Li S. Pilot diesel-ignited ammonia dual fuel low-speed marine engines: A comparative analysis of ammonia premixed and high-pressure spray combustion modes with CFD simulation. Renew Sustain Energy Rev 2023;173:113108. https://doi.org/10.1016/j.rser.2022.113108.

[10] Bayraktar M, Yüksel O. Analysis of the nuclear energy systems as an alternative propulsion system option on commercial marine vessels by utilizing the SWOT-AHP method. Nucl Eng Des 2023;407:112265. https://doi.org/10.1016/j.nucengdes.2023.112265.

[11] Ryu BR, Duong PA, Kang H. Comparative analysis of the thermodynamic performances of solid oxide fuel cell–gas turbine integrated systems for marine vessels using ammonia and hydrogen as fuels. Int J Nav Archit Ocean Eng 2023;15:100524. https://doi.org/10.1016/j.ijnaoe.2023.100524.

[12] de Souza TAZ, Coronado CJR, Silveira JL, Pinto GM. Economic assessment of hydrogen and electricity cogeneration through steam reforming-SOFC system in the Brazilian biodiesel industry. J Clean Prod 2021;279:123814. https://doi.org/10.1016/j.jclepro.2020.123814.

[13] van Veldhuizen BN, Zera E, van Biert L, Modena S, Visser K, Aravind PV. Experimental evaluation of a solid oxide fuel cell system exposed to inclinations and accelerations by ship motions. J Power Sources 2023;585:233634. https://doi.org/10.1016/j.jpowsour.2023.233634.

[14] Bayraktar M. Investigation of alternative fuelled marine diesel engines and waste heat recovery system utilization on the oil tanker for upcoming regulations and carbon tax. Ocean Eng 2023;287:115831. https://doi.org/10.1016/j.oceaneng.2023.115831.

[15] Liu L, Wu J, Liu H, Wu Y, Wang Y. Study on marine engine combustion and emissions characteristics under multi-parameter coupling of ammonia-diesel stratified injection mode. Int J Hydrogen Energy 2023;48:9881–94. https://doi.org/10.1016/j.ijhydene.2022.12.065.

[16] Çolak K, Ölmez H. Thermodynamic and feasibility analysis of using diesel generator exhaust gases for ship main engine preheating at port periods. Appl Therm Eng 2023;235:121429. https://doi.org/10.1016/j.applthermaleng.2023.121429.

[17] Liu X, Quang Nguyen M, He M. Performance analysis and optimization of an electricity-cooling cogeneration system for waste heat recovery of marine engine. Energy Convers Manag 2020;214:112887. https://doi.org/10.1016/j.enconman.2020.112887.

[18] De Robbio R, Cameretti MC, Palomba M, Tuccillo R, Mancaruso E. CFD Analysis of the Injection Strategy of a Dual Fuel Compression Ignition Engine Supplied with Hydrogen, SAE Technical Paper 2023-24-0064, 2023, doi:10.4271/2023-24-0064.

[19] Altinkurt MD, Merts M, Tunér M, Turkcan A. Effects of split diesel injection strategies on combustion, knocking, cyclic variations and emissions of a natural gas-diesel dual fuel medium speed engine. Fuel 2023;347:128517. https://doi.org/10.1016/j.fuel.2023.128517.

[20] Hyvättinen H, Hildén M. Environmental policies and marine engines—effects on the development and adoption of innovations. Mar Policy 2004;28:491–502. https://doi.org/10.1016/j.marpol.2004.01.001.

[21] Pinto GM, da Costa RBR, de Souza TAZ, Rosa AJAC, Raats OO, Roque LFA, et al. Experimental investigation of performance and emissions of a CI engine operating with HVO and farnesane in dual-fuel mode with natural gas and biogas. Energy 2023;277:127648. https://doi.org/10.1016/j.energy.2023.127648.

[22] Xiong Q, Wan Z, Liu L, Zhao B. Numerical analysis of combustion process and pressure oscillation phenomena in low-pressure injection natural gas/diesel dual fuel low speed marine engine. Thermal Science and Engineering Progress 2023;42:101913. https://doi.org/10.1016/j.tsep.2023.101913.

[23] Zhang Z, Lv J, Li W, Long J, Wang S, Tan D, et al. Performance and emission evaluation of a marine diesel engine fueled with natural gas ignited by biodiesel-diesel blended fuel. Energy 2022;256:124662. https://doi.org/10.1016/j.energy.2022.124662.

[24] Cavalcanti EJC. Energy, exergy and exergoenvironmental analyses on gas-diesel fuel marine engine used for trigeneration system. Appl Therm Eng 2021;184:116211. https://doi.org/10.1016/j.applthermaleng.2020.116211.

[25] Papagiannakis RG, Rakopoulos CD, Hountalas DT, Rakopoulos DC. Emission characteristics of high speed, dual fuel, compression ignition engine operating in a wide range of natural gas/diesel fuel proportions. Fuel 2010;89:1397–406. https://doi.org/10.1016/j.fuel.2009.11.001.

[26] Xiang L, Theotokatos G, Ding Y. Parametric investigation on the performance-emissions trade-off and knocking occurrence of dual fuel engines using CFD. Fuel 2023;340:127535. https://doi.org/10.1016/j.fuel.2023.127535.

[27] Hassan Q, Sameen AZ, Salman HM, Jaszczur M, Al-Jiboory AK. Hydrogen energy future: Advancements in storage technologies and implications for sustainability. J Energy Storage 2023;72:108404. https://doi.org/10.1016/j.est.2023.108404.

[28] Seyam S, Dincer I, Agelin-Chaab M. Investigation and comparative evaluation of a hybridized marine engine powered by eco-friendly fuels including hydrogen. Int J Hydrogen Energy 2023;48:4812–29. https://doi.org/10.1016/j.ijhydene.2022.11.008.

[29] Carlson EL, Pickford K, Nyga-Łukaszewska H. Green hydrogen and an evolving concept of energy security: Challenges and comparisons. Renew Energy 2023;219:119410. https://doi.org/10.1016/j.renene.2023.119410.

[30] Hosseini SH, Tsolakis A, Alagumalai A, Mahian O, Lam SS, Pan J, et al. Use of hydrogen in dual-fuel diesel engines. Prog Energy Combust Sci 2023;98:101100. https://doi.org/10.1016/j.pecs.2023.101100.

[31] Tan D, Wu Y, Lv J, Li J, Ou X, Meng Y, et al. Performance optimization of a diesel engine fueled with hydrogen/biodiesel with water addition based on the response surface methodology. Energy 2023;263:125869. https://doi.org/10.1016/j.energy.2022.125869.

[32] Zhang Z, Lv J, Xie G, Wang S, Ye Y, Huang G, et al. Effect of assisted hydrogen on combustion and emission characteristics of a diesel engine fueled with biodiesel. Energy 2022;254:124269. https://doi.org/10.1016/j.energy.2022.124269.

[33] Gholami A, Jazayeri SA, Esmaili Q. A detail performance and CO2 emission analysis of a very large crude carrier propulsion system with the main engine running on dual fuel mode using hydrogen/diesel versus natural gas/diesel and conventional diesel engines. Process Saf Environ Prot 2022;163:621–35. https://doi.org/10.1016/j.psep.2022.05.069.

[34] Atelge MR. Experimental study of a blend of Diesel/Ethanol/n-Butanol with hydrogen additive on combustion and emission and exegetic evaluation. Fuel 2022;325:124903. https://doi.org/10.1016/j.fuel.2022.124903.

[35] Pan H, Pournazeri S, Princevac M, Miller JW, Mahalingam S, Khan MY, et al. Effect of hydrogen addition on criteria and greenhouse gas emissions for a marine diesel engine. Int J Hydrogen Energy 2014;39:11336–45. https://doi.org/10.1016/j.ijhydene.2014.05.010.

[36] Pinto GM, de Souza TAZ, da Costa RBR, Roque LFA, Frez GV, Coronado CJR. Combustion, performance and emission analyses of a CI engine operating with renewable diesel fuels (HVO/FARNESANE) under dual-fuel mode through hydrogen port injection. Int J Hydrogen Energy 2023;48:19713–32. https://doi.org/10.1016/j.ijhydene.2023.02.020.

[37] Mallouppas G, Yfantis EA, Frantzis C, Zannis T, Savva PG. The effect of hydrogen addition on the pollutant emissions of a marine internal combustion engine genset. Energies (Basel) 2022;15:7206. https://doi.org/10.3390/en15197206.

[38] Pham VC, Kim J-S, Lee W-J, Choi J-H. Effects of hydrogen mixture ratio and scavenging air temperature on combustion and emission characteristics of a 2-stroke marine engine. Energy Rep 2023;9:195–216. https://doi.org/10.1016/j.egyr.2022.11.207.

[39] Cardoso JS, Silva V, Rocha RC, Hall MJ, Costa M, Eusébio D. Ammonia as an energy vector: Current and future prospects for low-carbon fuel applications in internal combustion engines. J Clean Prod 2021;296:126562. https://doi.org/10.1016/j.jclepro.2021.126562.

[40] Rodríguez CG, Lamas MI, Rodríguez JdeD, Abbas A. Possibilities of ammonia as both fuel and NOx reductant in marine engines: a numerical study. J Mar Sci Eng 2022;10:43. https://doi.org/10.3390/jmse10010043.

[41] Leilei X, Chang Y, Treacy M, Zhou Y, Jia M, Bai X-S. A skeletal chemical kinetic mechanism for ammonia/N-heptane combustion. SSRN Electron J 2022. https://doi.org/10.2139/ssrn.4123952.

[42] Yousefi A, Guo H, Dev S, Liko B, Lafrance S. Effects of ammonia energy fraction and diesel injection timing on combustion and emissions of an ammonia/diesel dual-fuel engine. Fuel 2022;314:122723. https://doi.org/10.1016/j.fuel.2021.122723.

[43] Shin J, Park S. Numerical analysis for optimizing combustion strategy in an ammonia-diesel dual-fuel engine. Energy Convers Manag 2023;284:116980. https://doi.org/10.1016/j.enconman.2023.116980.

[44] Xu L, Xu S, Bai X-S, Repo JA, Hautala S, Hyvönen J. Performance and emission characteristics of an ammonia/diesel dual-fuel marine engine. Renew Sustain Energy Rev 2023;185:113631. https://doi.org/10.1016/j.rser.2023.113631.

[45] Li Z, Zhang Z, Fan Y, Li J, Wu K, Gao Z, et al. Fuel reactivity stratification assisted jet ignition for low-speed two-stroke ammonia marine engine. Int J Hydrogen Energy 2024;49:570–85. https://doi.org/10.1016/j.ijhydene.2023.08.256.

[46] Zhu J, Zhou D, Yang W, Qian Y, Mao Y, Lu X. Investigation on the potential of using carbon-free ammonia in large two-stroke marine engines by dual-fuel combustion strategy. Energy 2023;263:125748. https://doi.org/10.1016/j.energy.2022.125748.

[47] Li T, Zhou X, Wang N, Wang X, Chen R, Li S, et al. A comparison between low- and high-pressure injection dual-fuel modes of diesel-pilot-ignition ammonia combustion engines. J Energy Inst 2022;102:362–73. https://doi.org/10.1016/j.joei.2022.04.009.

[48] Hong C, Ji C, Wang S, Xin G, Wang Z, Meng H, et al. An experimental study of various load control strategies for an ammonia/hydrogen dual-fuel engine with the Miller cycle. Fuel Process Technol 2023;247:107780. https://doi.org/10.1016/j.fuproc.2023.107780.

[49] Hong C, Ji C, Wang S, Xin G, Qiang Y, Yang J. Evaluation of hydrogen injection and oxygen enrichment strategies in an ammonia-hydrogen dual-fuel engine under high compression ratio. Fuel 2023;354:129244. https://doi.org/10.1016/j.fuel.2023.129244.
[50] Wang Y, Zhou X, Liu L. Theoretical investigation of the combustion performance of ammonia/hydrogen mixtures on a marine diesel engine. Int J Hydrogen Energy 2021;46:14805–12. https://doi.org/10.1016/j.ijhydene.2021.01.233.
[51] Wang B, Yang C, Wang H, Hu D, Duan B, Wang Y. Study on injection strategy of ammonia/hydrogen dual fuel engine under different compression ratios. Fuel 2023;334:126666. https://doi.org/10.1016/j.fuel.2022.126666.
[52] Qian Y, Pei X, Zheng L, Mi S, Ju D, Zhou D, et al. Improving thermal efficiency of an ammonia-diesel dual-fuel compression ignition engine with the addition of premixed low-proportion hydrogen. Int J Hydrogen Energy 2024;58:707–16. https://doi.org/10.1016/j.ijhydene.2024.01.235.
[53] De Robbio R, Cameretti MC, Mancaruso E, Tuccillo R, Vaglieco BM. CFD Analysis of Different Methane/Hydrogen Blends in a CI Engine Operating in Dual Fuel Mode, SAE Technical Paper 2022-01-1056, 2022, doi:10.4271/2022-01-1056.
[54] Abagnale C, Cameretti MC, Ciaravola U, Tuccillo R, Iannaccone S. Dual Fuel Diesel Engine at Variable Operating Conditions: A Numerical and Experimental Study, SAE Technical Paper 2015-24-2411, 2015, doi:10.4271/2015-24-2411.
[55] Cameretti MC, Tuccillo R, De SL, Iannaccone S, Ciaravola U. A numerical and experimental study of dual fuel diesel engine for different injection timings. Appl Therm Eng 2016;101:630–8. https://doi.org/10.1016/j.applthermaleng.2015.12.071.
[56] Cameretti MC, De Robbio R, Tuccillo R. Performance Improvement and Emission Control of a Dual Fuel Operated Diesel Engine, SAE Technical Paper 2017-24-0066, 2017, doi:10.4271/2017-24-0066.
[57] Cameretti MC, De Robbio R, Tuccillo R, Pedrozo V, Zhao H. Integrated CFD-Experimental Methodology for the Study of a Dual Fuel Heavy Duty Diesel Engine, SAE Technical Paper 2019-24-0093, 2019, doi:10.4271/2019-24-0093.
[58] De Robbio R, Cameretti MC, Tuccillo R. Ignition and combustion modelling in a dual fuel diesel engine. Propul Power Res 2020;9:116–31. https://doi.org/10.1016/j.jppr.2020.02.001.
[59] De Robbio R, Cameretti MC, Mancaruso E, Tuccillo R, Vaglieco BM. CFD study and experimental validation of a dual fuel engine: effect of engine speed. Energies (Basel) 2021;14:4307. https://doi.org/10.3390/en14144307.
[60] De Robbio R, Cameretti MC, Mancaruso E, Tuccillo R, Vaglieco BM. Combined CFD - Experimental Analysis of the In-Cylinder Combustion Phenomena in a Dual Fuel Optical Compression Ignition Engine, SAE Technical Paper 2021-24-0012, 2021, doi:10.4271/2021-24-0012.
[61] Cameretti MC, De Robbio R, Mancaruso E, Palomba M. CFD study of dual fuel combustion in a research diesel engine fueled by hydrogen. Energies (Basel) 2022;15:5521. https://doi.org/10.3390/en15155521.
[62] García Valladolid P, Tunestål P, Monsalve-Serrano J, García A, Hyvönen J. Impact of diesel pilot distribution on the ignition process of a dual fuel medium speed marine engine. Energy Convers Manag 2017;149:192–205. https://doi.org/10.1016/j.enconman.2017.07.023.
[63] Lamas MI, Rodríguez CG. Numerical model to study the combustion process and emissions in the Wärtsilä 6L 46 four-stroke marine engine. Polish Maritime Research 2013;20:61–6. https://doi.org/10.2478/pomr-2013-0017.
[64] Patankar SV. Numerical heat transfer and fluid flow. CRC Press; 2018. 10.1201/9781482234213.
[65] Yakhot V, Orszag SA. Renormalization-group analysis of turbulence. Phys Rev Lett 1986;57:1722–4. https://doi.org/10.1103/PhysRevLett.57.1722.
[66] Ranzi E, Frassoldati A, Stagni A, Pelucchi M, Cuoci A, Faravelli T. Reduced kinetic schemes of complex reaction systems: fossil and biomass-derived transportation fuels. Int J Chem Kinet 2014;46:512–42. https://doi.org/10.1002/kin.20867.
[67] Otomo J, Koshi M, Mitsumori T, Iwasaki H, Yamada K. Chemical kinetic modeling of ammonia oxidation with improved reaction mechanism for ammonia/air and ammonia/hydrogen/air combustion. Int J Hydrogen Energy 2018;43:3004–14. https://doi.org/10.1016/j.ijhydene.2017.12.066.
[68] Liang L, Stevens JG, Farrell JT. A dynamic multi-zone partitioning scheme for solving detailed chemical kinetics in reactive flow computations. Combust Sci Technol 2009;181:1345–71. https://doi.org/10.1080/00102200903190836.
[69] Han Z, Reitz RD. A temperature wall function formulation for variable-density turbulent flows with application to engine convective heat transfer modeling. Int J Heat Mass Transf 1997;40:613–25. https://doi.org/10.1016/0017-9310(96)00117-2.
[70] Reitz RD, Beale JC. Modeling spray atomization with the Kelvin-Helmholtz / Rayleigh-Taylor hybrid model. Atom Sprays 1999;9:623–50. https://doi.org/10.1615/AtomizSpr.v9.i6.40.
[71] Ra Y, Reitz RD. A vaporization model for discrete multi-component fuel sprays. Int J Multiph Flow 2009;35:101–17. https://doi.org/10.1016/j.ijmultiphaseflow.2008.10.006.
[72] Park H, Shim E, Bae C. Injection strategy in natural gas-diesel dual-fuel premixed charge compression ignition combustion under low load conditions. Engineering 2019;5:548–57. https://doi.org/10.1016/j.eng.2019.03.005.